Spin-glass-like state and reversible room-temperature magnetocaloric effect in double distorted perovskites Nd(Cu_3 − −xMn_x)Mn_4O_12

Qiang Zhang, Yohann Bréard, Vincent Hardy

Spin glass like state and reversible room-temperature magnetocaloric effect in double distorted perovskites $Nd(Cu_{3-x}Mn_x)Mn_4O_{12}$

Qiang Zhang[1-2*], Yohann Bréard[1], and Vincent Hardy[1]

[1]Laboratoire CRISMAT, UMR 6508, CNRS ENSICAEN, 6 Boulevard du Maréchal Juin, F-14052 Caen Cedex 4, France

[2]Neutron Scattering Division, Oak Ridge National Laboratory, Oak Ridge, Tennessee 37831, USA

Abstract

The preparation, complex magnetic properties and room-temperature magnetocaloric effect in $Nd(Cu_{3-x}Mn_x)Mn_4O_{12}$ with cation distribution $(Nd)_A(Cu_{3-x}^{2+x}Mn_x^{3+})_{A'}(Mn_{1+x}^{3+}Mn_{3-x}^{4+})_B O_{12}^{2-}$ (x=1 and 1.5) have been reported. Both compounds show a sharp paramagnetic-ferromagnetic (FM) transition at T_C of 300 K and 280 K, respectively. The substitution of Cu by Mn at A' site induces the emergence of a spin glass state below ≈ 63 K for x= 1 and ≈ 72 K for x=1.5 compound. Another antiferromagnetic-like magnetic transition is also observed in both compounds at 23 and 28 K, respectively, which is discussed as the antiferromagnetic coupling between Nd at the A' site and (Mn^{3+}/ Mn^{4+}) at the B site. These two compounds exhibit room-temperature magnetocaloric effect. For a small field of 2 T, the maximum magnetic entropy changes $-\Delta S_M$ are 1.5 J/kg K at 300 K and 1.4 J/kg K at 280 K, respectively. Moreover, the $-\Delta S_M$(T) curves show an asymmetric distribution, resulting in high refrigerant capacity values for both compounds. We further demonstrate the distinct roles of A'-site and B-site spins on the magnetic properties and the origin of the spin glass like state in double distorted perovskites $Ln(Cu_{3-x}Mn_x)Mn_4O_{12}$ family of compounds.

*Correspondence should be addressed to Q.Z.~(email: zhangq6@ornl.gov)

1. Introduction

The $AA'_3Mn_4O_{12}$ family[1] (A can be monovalent, divalent or trivalent, while A' is Cu^{2+} or Mn^{3+}) with double distorted perovskite-like structure exhibits rich physical properties, such as low-field magnetoresistance[1,3], half metallicity[4], multiferroicity[5]. The crystal structure has the particularity of containing 1:3 ordered A and A' cations in a 2 $\mathbf{a_0}$×2 $\mathbf{a_0}$×2 $\mathbf{a_0}$ cubic unit cell of *Im-3* symmetry ($\mathbf{a_0}$ is the unit cell of the ideal perovskite). The compounds in this family also have the novelty of involving Jahn-Teller cation Cu^{2+} or Mn^{3+} at A' site, which distorts the usual cubo-octahedral sites of the perovskite to a nearly square oxygen environment. Among them, $CaCu_3Mn_4O_{12}$ and its derivatives have received the most intensive studies since 1970s.[1-5] $CaCu_3Mn_4O_{12}$ is a ferrimagnet with a Curie temperature T_C of 355 K and a high saturation magnetization (M_S) of ~ 9 μ_B/f.u. Relatively little attention has been paid to the $LnA'_3Mn_4O_{12}$ systems where Ln is a magnetic lanthanide (Pr, Nd, Sm, Eu, Gd, Dy, Ho, Er, Tm, Yb, and Lu)[6-9]. One obstacle is probably that the preparation of such compounds usually requires high pressure (>2 GPa) and/or KClO4 as oxidizing agent. A good advance in the synthesis is that Retuerto *e.t*[9] prepared the $Ln(Cu_{3-x}Mn_x)Mn_4O_{12}$ (Ln= Pr and Nd, x=1 and 2) compounds using web-chemistry technique followed by the treatment at a modest-pressure of 200 bar in O_2. Nevertheless, there are relatively large amount of impurity phases above 20 % when x increases to 2 and the samples exhibit very smooth magnetic transitions near T_C.

Compared with $CaCu_3Mn_4O_{12}$, these $LnA'_3Mn_4O_{12}$ compounds have two distinct features: 1). The involvements of magnetic Ln^{3+} ions imply extra exchange interactions among A site (Ln^{3+}), A' site (Cu^{2+}) and B site (Mn^{4+}/Mn^{3+}), which may lead to more complex ground state; 2). They have a higher ferrimagnetic (FI) T_C (>370 K to 430 K) and a larger M_S ($\geq$ 10 μ_B/f.u, except ~ 8 μ_B/f.u in $SmCu_3Mn_4O_{12}$)[6,8], which is

beneficial for investigating the magnetocaloric effect (MCE) used for magnetic refrigeration and also provides a wider temperature window to tailor MCE to be around room temperature (RT) by the elemental substitution. To improve the magnetocaloric properties, it is of importance to synthesize the samples with good purity and sharp magnetic transition since the MCE is proportional to $|\frac{\partial M}{\partial T}|$[10,11]. Furthermore, it turns out that the partial substitution of Cu^{2+} by Mn^{3+} at A' site in $LnA'_3Mn_4O_{12}$ increases the valence mixing of Mn^{3+} and Mn^{4+} at B site[7-9], which may lead to interesting magnetic properties. In addition, due to the complex cation distributions in $LnA'_3Mn_4O_{12}$, it would be of importance to shed light on the roles of the A-site magnetic Ln^{3+}, A'-site (Cu^{2+}/Mn^{3+}) and B-site (Mn^{3+}/ Mn^{4+}) spins in their magnetic properties. Motivated by these features, we report the synthesis, magnetic properties and RT magnetocaloric effect in $Nd(Cu_{3-x}Mn_x)Mn_4O_{12}$ (x=1 and 1.5) compounds.

2. Experimental section

The polycrystalline $NdCu_3Mn_4O_{12}$ was usually synthesized using high-pressure (2 Gpa) or hydrothermal method.[2] Recently, Retuerto *et al.*[9] prepared the $Nd(Cu_{3-x}Mn_x)Mn_4O_{12}$ (x=1 and 2) compounds using web-chemistry technique followed by the treatment at a modest-pressure of 200 bar in O_2, with large secondary phases: 15.4 % of $NdMn_2O_5$ and 9.3 % of Mn_2O_3 for x=2 sample. Here, we succeeded in the preparation of $Nd(Cu_{3-x}Mn_x)Mn_4O_{12}$ (x=1 and 1.5) compounds with higher purity by a combined use of the sel-gel method and a relatively low O_2 pressure of 120 bar. Stoichiometric amounts of high-purity Nd_2O_3, CuO and $Mn(NO_3)_2.4H_2O$ starting materials were dissolved in nitric acid (35%) resulting in a transparent solution. Suitable amounts of citric acid as the chelating agent and polyethylene glycol were

added into the reactor and mixed thoroughly. Note that we added the polyethylene glycol to help in forming a network of cations from the precursor solution, which enables phase formation at relatively low temperatures/pressure. Then, the ethylenediamine was added until the solution became basic, as tested by litmus paper. A very homogenous gel was achieved after the heating process at 100 ^{o}C and black powder was obtained after the organic components were decomposed at 300^{o}C. Finally, the obtained powder was pressed into pellets and synthesized at 900 ^{o}C for 50 h under the O_2 pressure of 120 bar.

The structural characterization has been carried out by means of a Panalytical Xpert Pro diffractometer using Cu K_α radiations. The structural Rietveld refinements were performed using FullProf program[12] incorporated in the WinPLOTR Package. The frequency dependence of the *ac* susceptibility and *dc* temperature/field dependence of magnetization were recorded by means of an extraction technique in a Physical Properties Measurement System (PPMS, Quantum design).

3. Results and Discussion

3.1 crystallographic structure

Rietveld refinement have been performed on both polycrystalline samples of the solid solution $Nd(Cu_{3-x}Mn_x)Mn_4O_{12}$ (x = 1 and 1.5), as shown in Fig. 1 (a) and (b). Both structures of $NdCu_{3-x}Mn_xMn_4O_{12}$ (x = 1 and 1.5), were very well refined in the aristotype *Im-3* space group with a doubling of the cell parameter compared to the one of the ideal perovskites (Table I). A minor amount of $NdMn_2O_5$ for x=1 sample and a little larger amount (less than 2% in mass) of $NdMn_2O_5$ have been detected as secondary

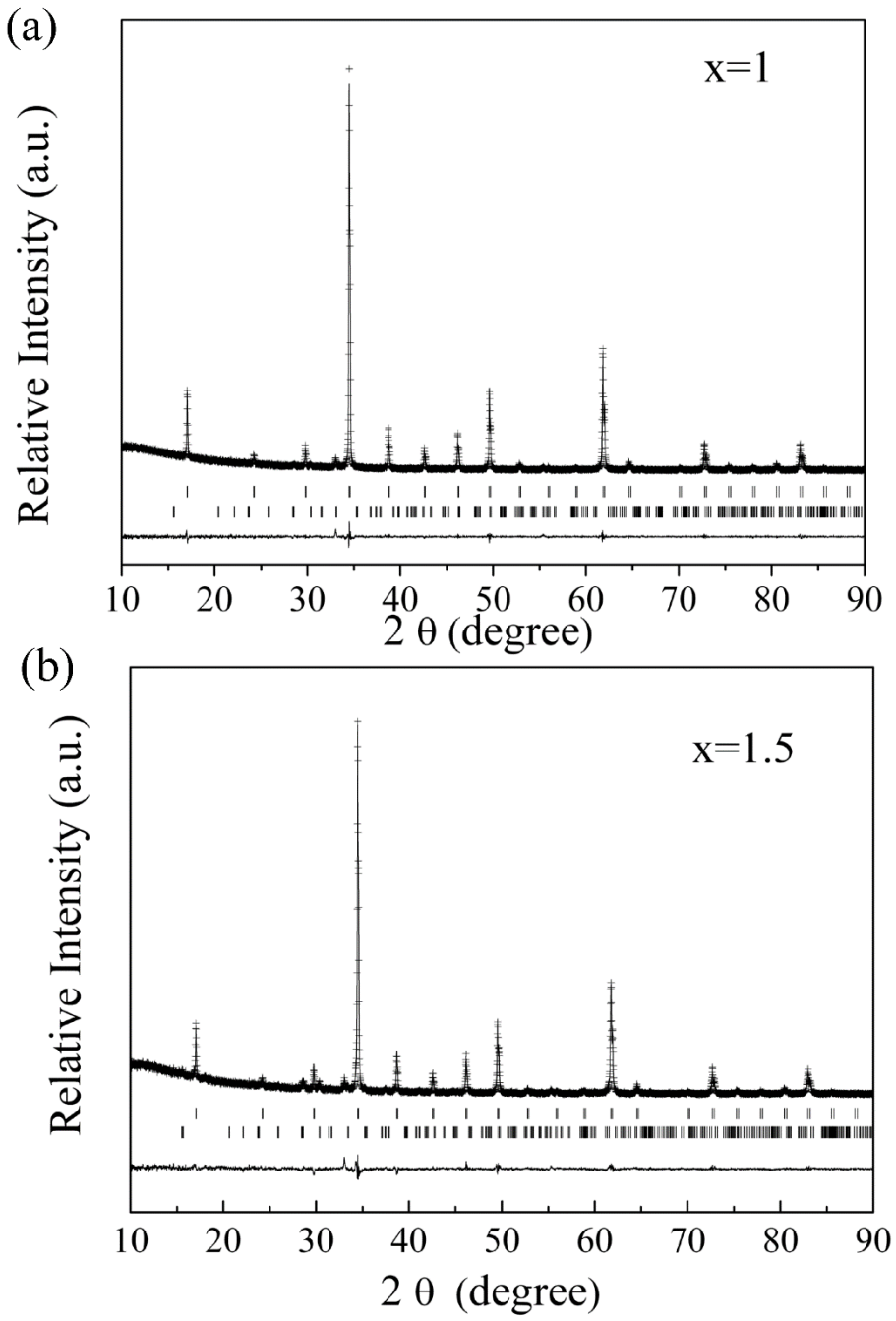

Fig. 1. Experimental (crosses), calculated (solid line) and difference (below) x-ray powder diffraction pattern of $NdCu_{3-x}Mn_xMn_4O_{12}$ for (a) x=1 and (b) x=2 determined at RT. The vertical bars are the Bragg angle positions for the main phase (upper) and the secondary phase $NdMn_2O_5$ (lower).

phase that is consequently introduced for the calculations for both samples. These refinements confirm the ordering of the A and A' cations (Nd and Cu/Mn_1) and the distortion of the oxygen framework, as shown in Fig. 2 with a drawing of the 3-D structure using the refinement results of $NdCu_2Mn_5O_{12}$. Any attempts to introduce order between Cu and Mn_1 atoms were unsuccessful. Whatever x, these two species are randomly distributed over the A' site in the square environment of oxygen.

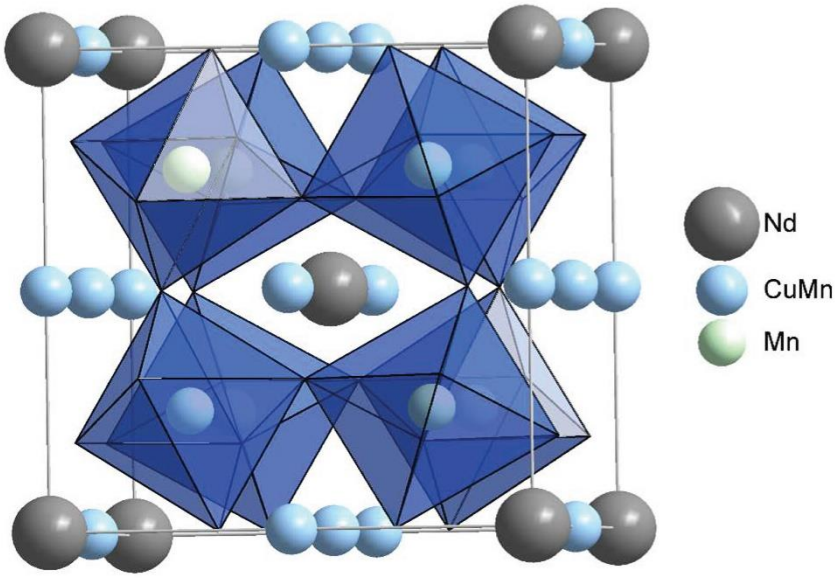

Fig. 2. A 3D view of the crystallographic structure of $Nd(Cu_{3-x}Mn_x)Mn_4O_{12}$ compounds obtained from the X-ray refinement of x=1 compound.

Despite the modest sensitivity of X-ray to their localization, the oxygen positions have been refined with a rather good value of their thermal displacements (Table I). One can note that whatever x, the distance between oxygen and Mn_2 atoms (which are lying on the octahedral site) remains unchanged while the distance between

A' cations (Cu/Mn) and oxygen atoms increase as x increases. As the manganese content increase, the tilting of the octahedral decrease and no change of the oxidation state of Mn_2 atoms seems to be observed. The angle Mn_2-O-Mn_2 tends to reach 180° which reinforces these interactions.

Table I. Structural parameters of $Nd(Cu_{3-x}Mn_X)Mn_4O_{12}$ (x =1 first line and x =1.5 second line) at room temperature obtained from X ray powder diffraction data.

S.G. I-3m (#204)					
	χ^2	R_{Bragg}	a (Å)	$d_{Cu/Mn1-O}$(Å)	d_{Mn2-O} (Å)
X=1	1.34	1.83	7.34721(9)	1.950	1.951
X=1.5	1.88	3.48	7.3547(1)	1.943	1.971
	x	y	z	B	S.O.F.
Nd (2a)	0	0	0	0.450	1
				0.437	1
Cu/Mn_1 (6b)	0	1/2	1/2	0.623	0.66/0.33
				0.560	0.5/0.5
Mn_2 (8c)	1/4	1/4	1/4	0.701	1
				0.420	1
O (24g)	0	0.3035(6)	0.1788(6)	0.225	1
		0.3090(8)	0.1880(1)	0.516	1

3.2 Magnetic transitions and the spin glass like state

The temperature dependence of the zero-field-cooled (ZFC) and field-cooled (FC) magnetization of $Nd(Cu_2Mn)Mn_4O_{12}$ and $Nd(Cu_{1.5}Mn_{1.5})Mn_4O_{12}$, is shown in Fig. 3. The impurity phase of $NdMn_2O_5$ exhibits successive magnetic transitions[13-14] at $T_1 \approx 36$ K, $T_2 \approx 15$ K and $T_3 \approx 4$ K. The FC magnetization shows a rapid increase near $T_1 \approx 36$ K and pronounced peaks near 10 and 4 K. All those features were not observed in our FC magnetization, which excludes the effect of this magnetic impurity phase $NdMn_2O_5$ on the magnetizations in Fig. 3. With the decrease of the temperature, a rapid increase in both ZFC and FC curves occurs in these two compounds at around RT due to the suppressed paramagnetic-ferromagnetic transitions[9] by the substitution of Cu by

Mn. A sharp peak, observed at 300 K and 280 K in the derivative of the magnetization (dM/dT) curve, corresponds to T_C in $Nd(Cu_2Mn)Mn_4O_{12}$ and $Nd(Cu_{1.5}Mn_{1.5})Mn_4O_{12}$,

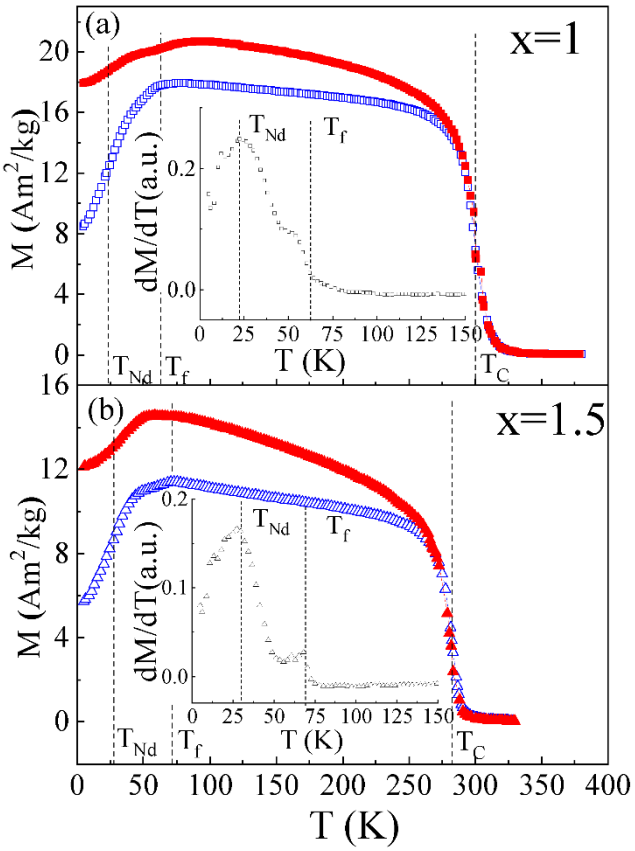

Fig. 3. The temperature dependence of the ZFC (open symbols) and FC (solid symbols) magnetizations in a field of 0.01 T in $Nd(Cu_{3-x}Mn_x)Mn_4O_{12}$ (x=1, 1.5) compounds. The insets of (a) and (b) show the first derivative of the ZFC magnetization with respect to the temperature for x=1 and 1.5 compounds, respectively.

respectively. As compared to the broad magnetic transitions spread ~ 90 K in x=1 and 2 compounds in previous report[9], the magnetic transitions in our samples occur in a much narrower window ~ 40 K in the same field of 0.1 T, indicative of a larger $|\frac{\partial M}{\partial T}|$. Note that while parent compound $NdCu_3Mn_4O_{12}$ is a ferrimagnetically ordered with dominant AFM interaction between $(Cu^{2+})_A$, site and $(Mn)_B$ site, it was reported that the

substitution of Cu^{2+} by Mn^{3+} at A' site induced a ferromagnetic order with a FM interaction between A' and B sites based on the neutron powder diffraction measurements[9]. There is a slight divergence between ZFC and FC curves in these two compounds below around T_C due to an effect of domain-wall pinning, leading to a larger magnetization upon field cooling process like in $(Cu_{3-x}Mn_x)Mn_4O_{12}$ compounds.[15] At low temperature, the magnetization in these two compounds becomes very complex: 1. Both ZFC and FC curves decrease as temperature decreases below ≈ 40 K; 2. The divergence between ZFC and FC curves becomes larger below ≈ 80 K; 3. The dM/dT curves show additional two peaks, as shown in the inset of Fig. 3 (a) and (b). To explore the nature of the low-temperature magnetic transitions, we investigated the frequency dependence of χ_{ac} for both compounds, with frequency ranging from 10^2 to 10^4 Hz, as shown in Fig. 4.

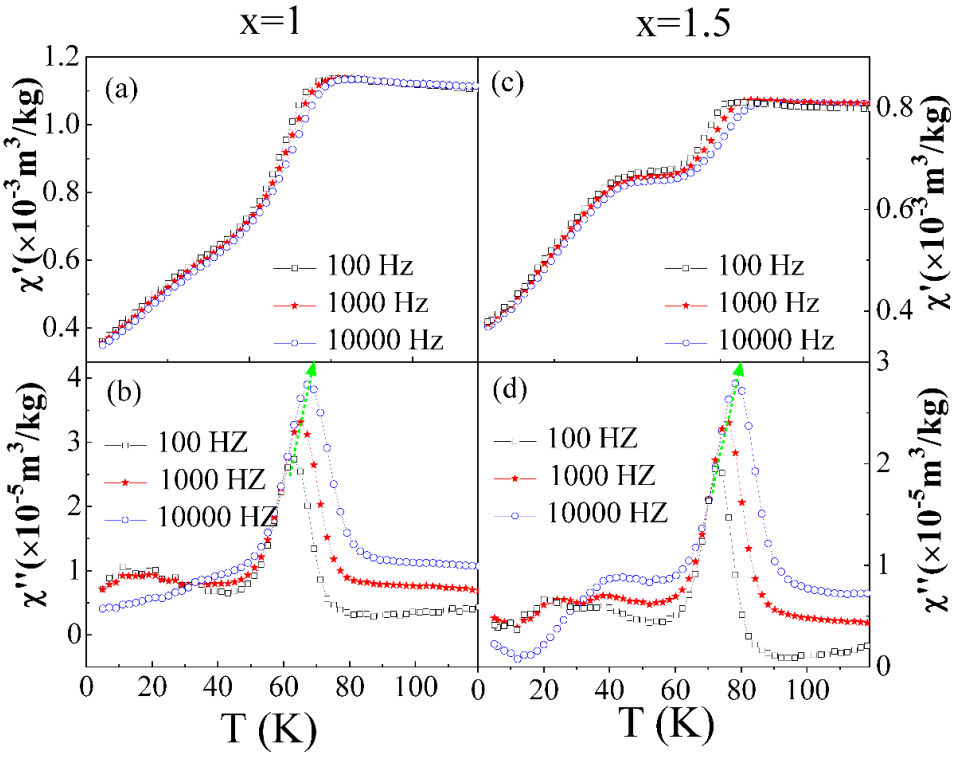

Fig. 4. Temperature dependences of (a) the in-phase (χ') and (b) the out-of-phase (χ'') *ac* susceptibility measured at different frequencies in x=1 compound; temperature

dependences of (c) the in-phase (χ') and (d) the out-of-phase (χ'') *ac* susceptibility measured at different frequencies in x=1.5 compound.

In $Nd(Cu_2Mn)Mn_4O_{12}$, the in-phase χ' shows the frequency-dependent behavior below ≈ 75 K. Moreover, the increase of frequency shifts the peak in the out-of-phase χ'' to higher temperature and increases the peak intensity simultaneously, which are typical behaviors for a spin-glass transition.[16-17] Using the phenomenological parameter $p = (\Delta T_f / T_f) / \Delta \log f$ where the characteristic freezing temperature T_f is the peak position in χ''(T), we found p is around 0.032, within the range (0.004-0.080) for typical spin-glass materials.[16] The T_f of 63 K at our lowest frequency (100 Hz) is consistent with the kink in the ZFC curve, close to the zero point in dM/dT. Therefore, we define the peak position in the χ''(T) at 100 Hz as the freezing temperature $T_g \approx$ 63 K. The similar spin-glass behavior is also observed in $Nd(Cu_{1.5}Mn_{1.5})Mn_4O_{12}$ compound with $p \approx 0.042$ and the spin glass transition was estimated to be $T_g \approx 72$ K.

In a pure spin glass like state, it is well known that upon cooling below T_g, the ZFC magnetization usually decreases, whereas the FC magnetization keeps unchanged or slight increasing[15]. However, with further decreasing the temperature below T_g, both ZFC and FC magnetization in x=1 and 1.5 compounds exhibits an anomalous decrease, indicative of an existence of an antiferromagnetic order or an antiferromagnetic interaction coming into play. Since such AFM ordering is not observed in $CaCu_{3-x}Mn_{4+x}O_{12}$ compounds, it should be driven by the existence of Nd in $Nd(Cu_{3-x}Mn_x)Mn_4O_{12}$. The AFM ordering within the Nd sublattice can be excluded since it usually occurs at very low temperatures (< 5 K). Instead, we argue that the AFM ordering is ascribed to the AFM interaction between Nd at the A site and (Mn^{3+}/ Mn^{4+}) at the B site. Such scenario shows some analogy to other Nd-based compounds such as

$NdFeO_3$[18] and $NdCrO_3$[19]. In $NdFeO_3$, the Nd moments are slightly induced by iron moments below $T \approx 25$ K prior to long-range Nd ordering below 1 K[18]. As for $NdCrO_3$, the Nd-Cr interaction starts to polarize the Nd moments at ≈ 11 K and Nd only becomes ordered below a very low temperature[19]. The low-temperature AFM transition temperatures (called T_{Nd} hereafter) for $Nd(Cu_2Mn)Mn_4O_{12}$ and $Nd(Cu_{1.5}Mn_{1.5})Mn_4O_{12}$ are determined to be 23 and 28 K, corresponding to the lowest peaks in the dM/dT and the inflection point in both ZFC and FC magnetizations as shown in Fig. 3 (a) and (b), respectively. It is worthwhile pointing out that an AFM transition between Tb at A site and (Mn^{3+}/ Mn^{4+}) at B site was reported in $TbCu_3Mn_4O_{12}$ below ~ 75 K[20]. The AFM alignments of Nd and B-site spins have also been found in $NdCu_3(Mn_3Fe)O_{12}$ below ~ 80 K[9]. The absence of pure antiferromagnetic peaks in the neutron powder diffractions on $Nd(Cu_{3-x}Mn_x)Mn_4O_{12}$ (x=1 and 2) samples in *Ref.* 9 is probably due to due to weaker antiferromagnetic coupling as indicated by a weaker decrease of the FC magnetization below ~ 40 K in their samples, a weak moment of Nd (no more than 1 μ_B) and the poor statistics of the neutron data.

The spin glass state in $Nd(Cu_{3-x}Mn_x)Mn_4O_{12}$ has never been reported previously. To further investigate such spin glass state, the temperature dependence of the ZFC and FC at different fixed magnetic fields was measured. As shown in Fig. 5 (a), the divergence between ZFC and FC curves in x=1.5 compound is suppressed significantly with the increase of the magnetic field, and disappears when the magnetic field is at and above 0.3 T. The decrease for both ZFC and FC curves below ≈ 30 K for x= 1.5 may results from the AFM coupling between Nd at A site and (Mn^{3+}/ Mn^{4+}) at B site. In a high field of 5 T, the anomalous decrease below T_{Nd} disappeared and instead, a gradual increase was observed. This indicates that the AFM coupling between Nd at A site and (Mn^{3+}/ Mn^{4+}) at B site is suppressed by the external field of 5 T. In addition,

the Fig. 5 (b) shows the isothermal magnetizations for x=1 and x=1.5 with maximum

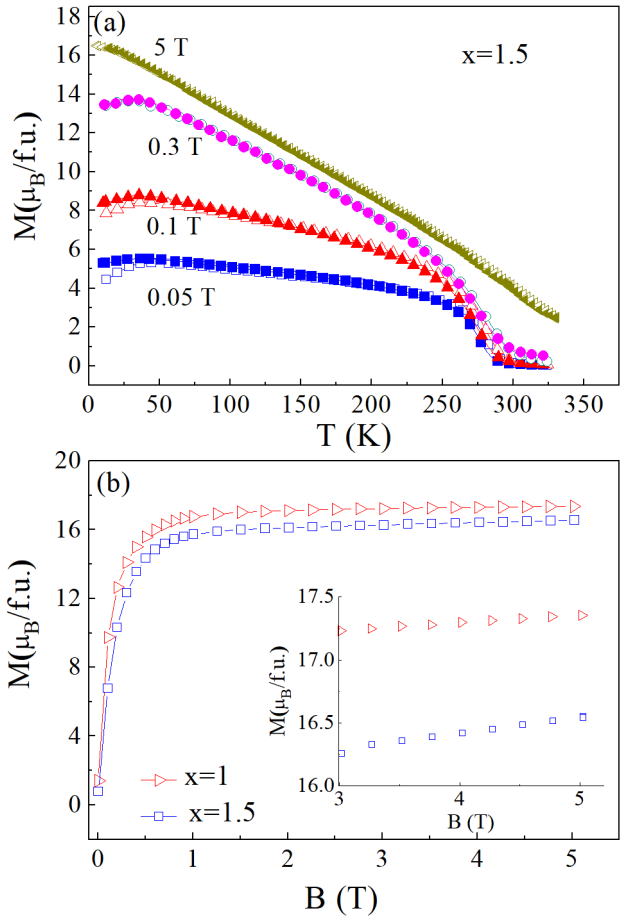

Fig. 5**. (a)** Temperature dependences of the ZFC (open symbols) and FC (solid symbols) magnetization measured in different dc fields for x=1.5 compound. (b) Magnetization curve recorded at 5 K in the $Nd(Cu_{3-x}Mn_x)Mn_4O_{12}$ (x=1, 1.5) compounds. The inset shows the zoomed-in figure under high fields from 3 T to 5 T

magnetization of 17.3 and 16.5 u_B at 5 T, respectively. The magnetization shows a rapid increase at low fields (< 1 T) as a typical ferromagnetic behavior. However, the magnetization keeps increasing slowly with further increasing fields without the saturation up to 5 T due to the field-induced polarization of spins (see inset of Fig. 5(b)) as expected in a spin glass state[21]. This indicates that both compounds show a mixed feature of the ferromagnetism and spin glass under high fields, similar to the feature

observed in Ni-Mn[21] or $La_{0.5}Sr_{0.5}CoO_3$[22-23]. Thus, at zero field, the ground state of both compounds is a coexistence of a spin glass like state with the complicated magnetic order involving FM coupling between A' and B site and AFM coupling between A-site Nd and B-site ions. It should be noted that due to the coexistence of such weak spin glass like state with the dominant long-range FM order, it is very usual that no diffuse scattering indicated by the peak broadening is detectible to directly observe the spin glass like state by the neutron powder diffraction technology[9].

3.3 Roles of $(Mn^{3+}/Mn^{4+})_A$ and $(Cu^{2+}/Mn^{3+})_B$ spins in magnetic properties

The cation distribution of $CaCu_{3-x}Mn_{4+x}O_{12}$ was reported to be $(Ca^{2+})_A(Cu^{2+}_{3-x}Mn^{3+}_x)_{A'}(Mn^{3+}_xMn^{4+}_{4-x})_BO^{2-}_{12}$.[24] In contrast, the cation distribution in $NdCu_3Mn_4O_{12}$ is $(Nd^{3+})_A(Cu^{2+}_3)_{A'}(Mn^{3+}Mn^{4+}_3)_BO^{2-}_{12}$.[6] It has been reported[8-9] that the $(Cu)_{A'}$ moments are antiparallel to those of $(Mn^{3+}/Mn^{4+})_B$, forming the FI structure in $NdCu_3Mn_4O_{12}$ below T_C. The partial substitution of Cu by Mn at A' site in $Nd(Cu_{3-x}Mn_x)Mn_4O_{12}$ increases the valence mixing of Mn^{3+} and Mn^{4+} at B site, leads to a more complex cation distribution of $(Nd^{3+})_A(Cu^{2+}_{3-x}Mn^{3+}_x)_{A'}(Mn^{3+}_{1+x}Mn^{4+}_{3-x})_BO^{2-}_{12}$,[4,6] with ferromagnetic arrangements between $(Cu^{2+})_{A'}$ and $(Mn^{3+}/Mn^{4+})_B$ driven by the substitution of Cu by Mn[9] and possible antiferromagnetic arrangements between $(Nd^{3+})_{A'}$ and $(Mn^{3+}/Mn^{4+})_B$. Simultaneously, it was proposed[9] that the increase of the substitution may induce an antiferromagnetic coupling within B site, which could interpret the decrease of the global moment as x increases from 1 to 1.5 compound here. Interestingly, the comparison between $CaCu_{3-x}Mn_{4+x}O_{12}$ and $Nd(Cu_{3-x}Mn_x)Mn_4O_{12}$ series may provide an opportunity to separate the effect of A'-site and B-site spins on the magnetic properties in $LnCu_{3-x}Mn_{4+x}O_{12}$.

To pursue this, we show the ratio $Mn^{3+}/(Mn^{3+}+Mn^{4+})_B$ at B site as a function of the ratio $Mn^{3+}/(Cu^{2+}+Mn^{3+})_{A'}$ at A' site (bottom axis) and x value (top

axis) in $(Nd^{3+})_A(Cu^{2+}_{3-x}Mn^{3+}_x)_{A'}(Mn^{3+}_{1+x}Mn^{4+}_{3-x})_BO^{2-}_{12}$ in Fig. 6. The Curie

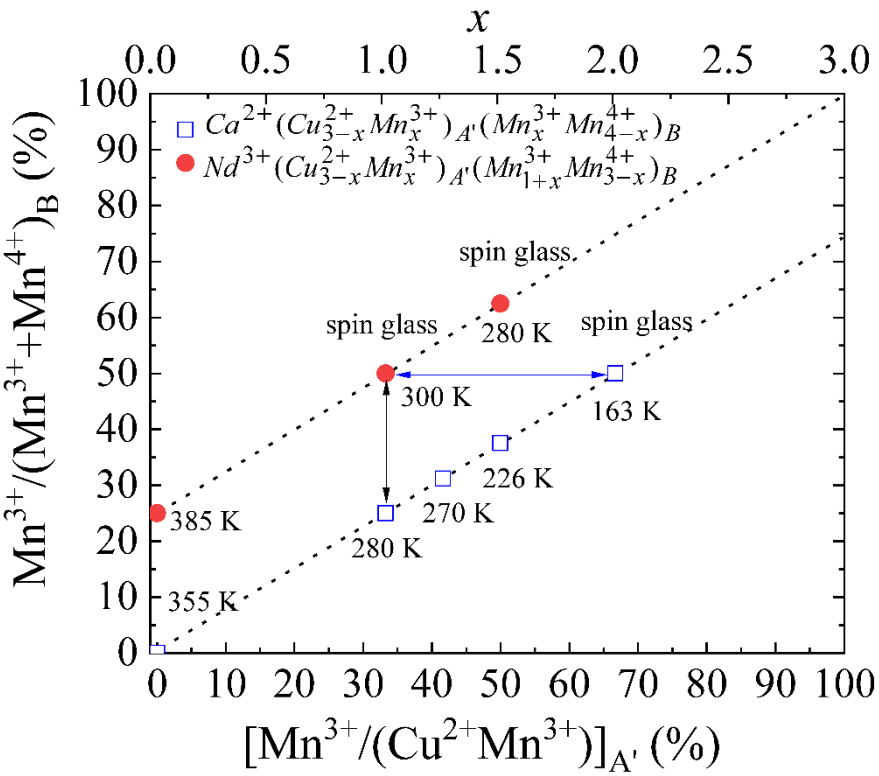

Fig. 6. (Color online) The ratio $Mn^{3+}/(Mn^{3+}+Mn^{4+})_B$ at B site as a function of the ratio $Mn^{3+}/(Cu^{2+}+Mn^{3+})_{A'}$ at A' site (bottom axis) and x value (top axis) in $(Ca^{2+})_A(Cu^{2+}_{3-x}Mn^{3+}_x)_{A'}(Mn^{3+}_xMn^{4+}_{4-x})_BO^{2-}_{12}$ and $(Nd^{3+})_A(Cu^{2+}_{3-x}Mn^{3+}_x)_{A'}(Mn^{3+}_{1+x}Mn^{4+}_{3-x})_BO^{2-}_{12}$

temperatures are added in the figure. A few interesting phenomena were observed. 1). If one compares x=1 in Nd-series, and x=2 in the Ca-series, the A'-site $Mn^{3+}/(Cu^{2+}+Mn^{3+})_{A'}$ ratio increases significantly shown as the horizontal arrows while the $Mn^{3+}/(Mn^{3+}+Mn^{4+})_B$ ratio at B site keeps the same. The magnitudes of magnetization at 5 T (close to saturation magnetization) for these two compounds are similar, 17.4 and 17.2 u_B, respectively. The main difference in the magnetic property is the rapidly reduced T_C from 280 K to 163 K. We therefore conclude that the A'-site $Mn^{3+}/(Cu^{2+}+Mn^{3+})_{A'}$ ratio plays a key role in controlling T_C via the governed magnetic interaction between A' and B sites no matter if it is ferromagnetic type in

$NdCu_{3-x}Mn_{4+x}O_{12}$ or antiferromagnetic type in ferrimagnetic $CaCu_{3-x}Mn_{4+x}O_{12}$. 2). For two vertical arrows for x=0 or 1 in both series of compounds, the A'-site ratios are unchanged as shown by the vertical lines but there are large differences in B-site $Mn^{3+}/(Mn^{3+}+Mn^{4+})_B$ ratio. The magnitudes of T_C are comparable due to similar A'-site $Mn^{3+}/(Cu^{2+}+Mn^{3+})_{A'}$ ratios. However, the magnitudes of magnetization at 5 T (close to saturation magnetization) are reduced from 17.4 u_B in x=1 of Nd-series to 14.6 u_B in x=1 of Ca-series. This indicates that the B-site $Mn^{3+}/(Mn^{3+}+Mn^{4+})_B$ ratio strongly determines the saturation moments. This can be interpreted by the different moment size between Mn^{3+} (~ 4 u_B) and Mn^{4+} (~ 3 u_B) spins, both of which are much larger than ~ 1 u_B for Nd^{3+} or Cu^{2+}. 3). The spin glass like state in the series of $CaCu_{3-x}Mn_{4+x}O_{12}$ is formed only when the substitution content (x) of Mn by Cu is increased to be 2 with T_g≈70 K. In contrast, the spin glass like state in $Nd(Cu_{3-x}Mn_x)Mn_4O_{12}$ exists when there is a low substitution (x≥1), as shown in Fig. 6. Note that the locations of T_g between x=2 in $CaCu_{3-x}Mn_{4+x}O_{12}$ is very close to those for x=1 and 1.5 in $Nd(Cu_{3-x}Mn_x)Mn_4O_{12}$ and the AFM coupling between Nd lattice and (Mn^{3+}/ Mn^{4+}) at B site is weak since T_{Nd} is much lower than T_g. Both could exclude the important role of Nd spins in the formation of the spin glass like state in $Nd(Cu_{3-x}Mn_x)Mn_4O_{12}$. Furthermore, compared to x≤1.5 in $CaCu_{3-x}Mn_{4+x}O_{12}$ without spin glass like state, the common feature in the x=2 in $CaCu_{3-x}Mn_{4+x}O_{12}$ and x≥1 in $Nd(Cu_{3-x}Mn_x)Mn_4O_{12}$ is that the B-site $Mn^{3+}/(Mn^{3+}+Mn^{4+})$ ratios are higher. Note that for x=1 (or 1.5) in $CaCu_{3-x}Mn_{4+x}O_{12}$ and $NdCu_{3-x}Mn_{4+x}O_{12}$, the A-site $Mn^{3+}/(Cu^{2+}/ Mn^{3+})$ ratios are the same, but the B-site $Mn^{3+}/(Mn^{3+}/ Mn^{4+})$ ratios in $NdCu_{3-x}Mn_{4+x}O_{12}$ are higher than those in $CaCu_{3-x}Mn_{4+x}O_{12}$ (see Fig. 6). All of these results unveil that the B-site Mn^{3+}/Mn^{4+} disorder plays a main role in the formation of the spin glass like state in both $CaCu_{3-x}Mn_{4+x}O_{12}$ and $Nd(Cu_{3-x}Mn_x)Mn_4O_{12}$ compounds.

3.4 Room-temperature magnetocaloric effect

The high magnetization and sharper magnetic transition in our samples than those reported previously[9] motivated us to investigate the magnetocaloric effect. The magnetic isotherms have been measured on $Nd(Cu_{3-x}Mn_x)Mn_4O_{12}$ (x=1 and 1.5) compounds and the representative curves of $Nd(Cu_2Mn)Mn_4O_{12}$ are shown in Fig. 7.

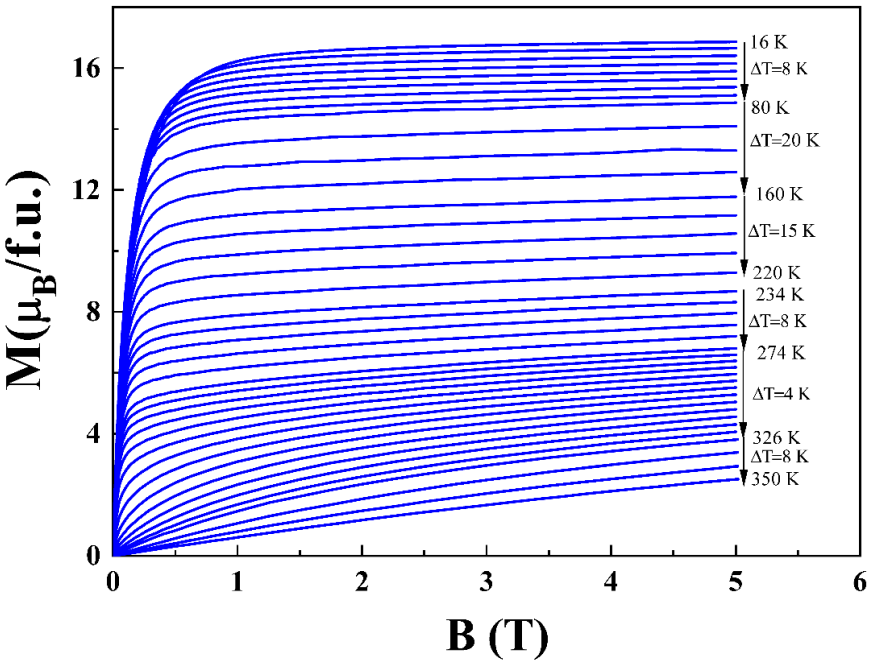

Fig. 7. (Color online) Series of magnetic isotherms recorded in the x = 1 compound in the temperature region of 16-350 K

There is no magnetic hysteresis between increasing-field and decreasing-field branches, suggesting that the FM-PM transition is a second-order magnetic transition. Accordingly, the isothermal entropy changes $-\Delta S_M$ can be calculated reliably *via* the Maxwell relation.[10]

$$\Delta S_M(T,\Delta B) = S_M(T,B) - S_M(T,0) = \int_0^B \left(\frac{\partial M}{\partial T}\right)_{B'} dB' \qquad (2)$$

Fig. 8 shows the $-\Delta S_M$(T) curves for $Nd(Cu_2Mn)Mn_4O_{12}$ and $Nd(Cu_{1.5}Mn_{1.5})Mn_4O_{12}$ as

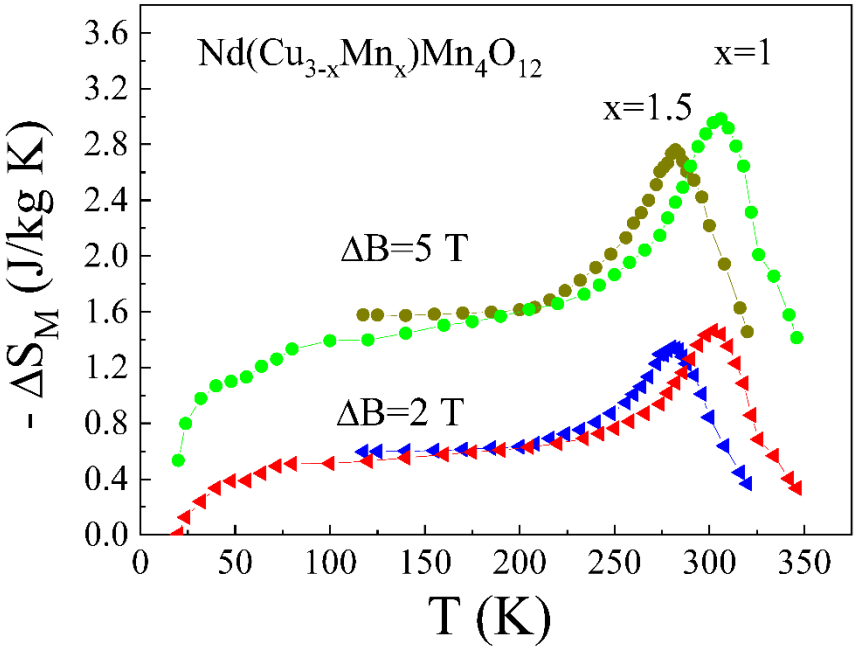

Fig. 8. (Color online) Temperature dependence of the isothermal entropy changes in $Nd(Cu_{3-x}Mn_x)Mn_4O_{12}$ (x = 1 and 1.5) compounds for field changes equal to 2 T and 5 T

a function of temperature for field changes (ΔB) of 2 T, 5 T. The maximum $-\Delta S_M$ values of the two compounds occur in the vicinity of their respective Curie temperatures of 300 and 280 K, showing the RT magnetocaloric effect. In Table II, we summarized the maximum $-\Delta S_M$ values for different field changes. For a field change of 5 T, the maximum $-\Delta S_M$ values are found to be 3.0 and 2.72 J/kg K for $Nd(Cu_2Mn)Mn_4O_{12}$ and $Nd(Cu_{1.5}Mn_{1.5})Mn_4O_{12}$, respectively. It can also be found that the $-\Delta S_M$(T) curves exhibit asymmetrical shape, i.e. the fact that the decrease on the low-T side of the peak is significantly slower than on the high-T side. This special feature is strongly different from the roughly symmetrical shape of $-\Delta S_M$(T) curves in the conventional perovskite magnetites.[10,25] but similar to that observed in $Ca(Cu_{3-x}Mn_x)Mn_4O_{12}$ compounds[15]. In

addition, there is one kink in the -ΔS_M(T) curves near the spin glass transition temperature T_g as shown for x=1 compound, indicating that the spin glass transition influences the isothermal entropy changes. The asymmetrical shape of the -ΔS_M(T) curves greatly enlarges the temperature span of MCE in $Nd(Cu_2Mn)Mn_4O_{12}$ and $Nd(Cu_{1.5}Mn_{1.5})Mn_4O_{12}$ due to the substitution-induced magnetic inhomogeneity at both the A' and B sites as discussed previously, which is favorable in operating modes like Active Magnetic Regeneration Refrigeration (AMRR)[26, 27] based on the development of a temperature gradient along the active material. To further illustrate this point, we evaluated the refrigerant capacity (RC) and δT_{FWHM}.

The RC values for reversible refrigeration[27, 28] can be obtained by numerically integrating the area under the -ΔS_M versus T curves, using the temperatures at half-maximum of the -ΔS_M peak as the integration limits $RC = \int_{T_{cold}}^{T_{hot}} \Delta S_M(T) \cdot dT$, here T_{hot} and T_{cold} are the corresponding two temperatures of half-maximum of the -ΔS_M peak. δT_{FWHM} is the difference between T_{hot} and T_{cold}, i.e., $\delta T_{FWHM} = T_{hot} - T_{cold}$. Alternatively, we also calculated the relative cooling power (RCP): $RCP = -\Delta S_M^{\max} \cdot \delta T_{FWHM}$.[25] We compared the magnetocaloric parameters in our two compounds to those in other excellent perovskite oxides and "reference" Gd in Table II. As compared to the "reference" Gd[30,33] with the second order transition, the maximum -ΔS_M values in $Nd(Cu_2Mn)Mn_4O_{12}$ and $Nd(Cu_{1.5}Mn_{1.5})Mn_4O_{12}$ are lower. Nevertheless, this can be compensated by the larger RC and δT_{FWHM} values in our compounds. Let us take $Nd(Cu_2Mn)Mn_4O_{12}$ exhibiting the maximum -ΔS_M well located at RT as one example for the detailed comparison. For ΔB= 2 T that can be realized by using a NdFeB permanent magnet, although -ΔS_M(T) in $Nd(Cu_2Mn)Mn_4O_{12}$ for

Table II. Comparison of magnetocaloric parameters in $Nd(Cu_{3-x}Mn_x)Mn_4O_{12}$ (x=1 and

2) with some of the best single perovskite manganites and the "reference" Gd around RT.

Material	ΔB (T)	T_{peak} (K)	$-\Delta S_M$ (J/kgK)	δT_{FWHM} (K)	RC (J/ kg)	RCP (J/ kg)	Reference
$La_{0.7}Ca_{0.25}Sr_{0.05}MnO_3$	2	279	4.5	15.5	—	70	29
$Nd(Cu_2Mn)Mn_4O_{12}$	2	302	1.5	81	87	122	This work
$Nd(Cu_{1.5}Mn_{1.5})Mn_4O_{12}$	2	280	1.4	100	91	140	This work
Gd	2	293	4.2	39.5	134.4	166	30
$Pr_{0.63}Sr_{0.37}MnO_3$	5	300	8.52	60	383	511	31
$La_{0.7}Ca_{0.20}Sr_{0.10}MnO_3$	5	308	7.45	50.2	—	374	32
$Nd(Cu_2Mn)Mn_4O_{12}$	5	306	3.0	182	360	546	This work
$Nd(Cu_{1.5}Mn_{1.5})Mn_4O_{12}$	5	283	2.72	196	492	739	This work
Gd	5	294	10.2	63	503	643	33

ΔB= 2 T is only 36% of the polycrystalline Gd, a large δT_{FWHM} value of 81 K is twice of the value of Gd (40 K)[30]. As a result, the RC value of 90 J/kg in $Nd(Cu_2Mn)Mn_4O_{12}$ reaches 66% of that of Gd. The reversible $-\Delta S_M$, wide working span and high RC values without hysteresis losses make $Nd(Cu_2Mn)Mn_4O_{12}$ and $Nd(Cu_{1.5}Mn_{1.5})Mn_4O_{12}$ interesting candidates for RT magnetic refrigeration.

4. Conclusion

In summary, the $Nd(Cu_2Mn)Mn_4O_{12}$ and $Nd(Cu_{1.5}Mn_{1.5})Mn_4O_{12}$ compounds involving less than 2% impurity with sharp magnetic transitions have been prepared by the combined use of sel-gel method and a relatively low O_2 pressure of 120 bar. The substitution of Cu by Mn tunes the ferromagnetic transitions to be around room temperature: 300 K for x= 1 and 280 K for x=1.5. With decreasing the temperature,

these two compounds enter a spin glass like state, followed by another antiferromagnetic transition due to the possible antiferromagnetic couplings between A'-site Nd and B-site (Mn^{3+}/Mn^{4+}) ions at lower temperatures. The (Mn^{3+}/Mn^{4+}) disorder at the B site contributes significantly to the formation of the spin glass like state in both compounds. We further reveal that the A'-site and B-site spins in $Nd(Cu_{3-x}Mn_x)Mn_4O_{12}$ play an important role in controlling T_C and saturation moments, respectively. The high moments and disorder-induced magnetic inhomogeneity of these two compounds lead to a reversible high refrigerant capacity over a wide temperature region. Our results indicate that $Nd(Cu_{3-x}Mn_x)Mn_4O_{12}$ (x=1 and 1.5) compounds are interesting materials for room-temperature magnetic refrigeration and for exploring peculiar magnetic properties.

Acknowledgments

This work has been primary supported by the European project "SOPRANO" under Marie Curie actions (Grant. No. PITN-GA- 2008-214040) and the CNRS project "Réfrigération Magnétique" within the frame of the "Programme Interdisciplinaire Energie". Q. Z. is supported by the Scientific User Facilities Division, Basic Energy Sciences, US DOE, at the late stage of this work.

*R*eferences

[1]Chenavas, J.; Joubert, M.; Marezio, J. C.; Bochu, B. The synthesis and crystal structure of $CaCu_3Mn_4O_{12}$: A new ferromagnetic-perovskite-like compound. *J. Solid State Chem.* **1975**, *14* 25.

[2]Vasil'ev A. N.; Volkova, O. S. New functional materials $AC_3B_4O_{12}$ (Review). Low Temp. Phys. **2007** *33,* 895.

[3]Zeng, Z.; Greenblatt, M.; Subramanian, M. A.; Subramanian, M. A. Large Low-Field Magnetoresistance in Perovskite-type $CaCu_3Mn_4O_{12}$ without Double Exchange. *Phys. Rev. Lett.* **1999** *82*, 3164.

[4]Lv, S.; Li, H.; Han, D.; Wu, Z.; Liu, X.; Meng, J. A better ferrimagnetic half-metal LuCu3Mn4O12: Predicted from first-principles investigation. *J. Magn. Magn. Mater*, **2011** *323,* 416.

[5]Johnson, R. D.; Chapon, L. C.; Khalyavin, D. D.; Manuel, P.; Radaelli, P. G.; Martin, C. Giant Improper Ferroelectricity in the Ferroaxial Magnet $CaMn_7O_{12}$. *Phys. Rev. Lett.* **2012** *108,* 067201.

[6]Bochu, B.; Joubert, J. C.; Collomb, A.; Ferrand, B.; D. Samaras, Ferromagnetic oxides $Ln^{3+}/Cu^3]Mn_4O_{12}$ (Ln = La TO Lu and Y). *J. Magn. Magn. Mater*. **1980** *15-18,* 1319.

[7]Samaras, D.; Bochu B.; Joubert, J. C.- Synthesis, composition, and magnetic properties of the ferrimagnetic $NdCu_{3-x}Mn_{4+x}O_{12}$ perovskite-like phases. *J. Solid State Chem.* **1984** *53,* 323.

[8]Sánchez-Benítez, J.; Alonso, J. A.; Falcón, H.; Martínez-Lope, M. J.; Andrés A. de.; Fernández-Díaz, M. T. Preparation under high pressures and neutron diffraction study of new ferromagnetic $RCu_3Mn_4O_{12}$ (R = Pr, Sm, Eu, Gd, Dy, Ho, Tm, Yb) perovskites. *J. Phys.: Condens. Matter.* **2005** *17,* S3063.

[9]Munoz, A.; Martinez-Lope, M. J.; Retuerto, M.; Falcon, H.; Alonso, J. A. Synthesis,

magnetic properties, and neutron diffraction study of the complex perovskites $R(Cu_{3-x}Mn_x)Mn_4O_{12}$ (R=Pr, Nd and x=1,2). *J. Appl. Phys.* **2008 104**, 083911.

[10]Gschneidner, Jr. K. A.; Pecharsky, V. K. Magnetocaloric Materials. *Annu. Rev. Mater. Sci.* **2000** *30,* 387.

[11]Zhang, Q.; Cho, J.H.; Li, B.; Hu, W.J.; Zhang, Z.D. Magnetocaloric effect in over a wide temperature range, *Appl. Phys. Lett.,* **2009** *94*, 182501.

[12]Rodr´ıguez-Carvajal, J. Recent advances in magnetic structure determination by neutron powder diffraction. *Phys. B: Condens. Matter,* **1993** *192,* 55-69.

[13]Chattopadhyay, S.; Balédent, V.; Auban-Senzier, P.; Pasquier, C.; Doubrovsky, C.; Greenblatt, M.; Foury-Leylekian, P. Thermodynamic and neutron diffraction studies on multiferroic $NdMn_2O_5$, *Physica B: Condensed Matter*, **2015** *460,* 214-217**.**

[14] Chattopadhyay, S.; Balédent, V.; Damay, F.; Gukasov, A.; Moshopoulou, E.; Auban-Senzier, P.; Pasquier, C.; André, G.; Porcher, F.; Elkaim, E.; Doubrovsky, C.; Greenblatt, M.; and Foury-Leylekian, P. Evidence of multiferroicity in $NdMn_2O_5$, *Phys. Rev. B,* **2016** *93,* 104406.

[15]Zhang, Q.; Br´eard, Y.; Guillou, F.; V. Hardy, Investigation of the magnetocaloric effect in double distorted perovskites $Cu(Cu_{3-x}Mn_x)Mn_4O_{12}$ ($1 \leq x \leq 2$): From standard ferrimagnetism to glassy ferrimagnetism. *Phys. Rev. B* **2011** *84,* 224430.

[16]Mydosh, A. J. *Spin Glasses: An Experimental Introduction (London: Taylor and Francis),* (1993).

[17]Bréard, Y.; Hardy, V.; Raveau, B.; Maignan, A.; Lin, H. J.; Jang, L. Y.; Hsieh H. H.; Chen, C. T. Spin-glass state induced by cobalt substitution in $CaRuO_3$. *J. Phys.: Condens. Matter.* **2007** *19,* 216212.

[18]Bartolomé, J.; Palacios, E.; Kuz'min, M. D.; Bartolomé, F.; Sosnowska, I.; Przeniosło, R.; Sonntag, R.; Lukina, M. M. Single-crystal neutron diffraction study of Nd magnetic

ordering in $NdFeO_3$ at low temperature. *Phys. Rev. B* **1997** *55,* 11432.

[19]Bartolomé, F.; Bartolomé, J.; Castro, M.; Melero, J. J. Specific heat and magnetic interactions in $NdCrO_3$ *Phys. Rev. B* **2000** *62,* 1058.

[20]Sánchez-Benitez, J.; Alonso, J. A.; de Andrés, A.; Martinez-Lope, M. J.; Martinez, J. L.; Muñoz, A. Peculiar Magnetic Behavior of the $TbCu_3Mn_4O_{12}$ Complex Perovskite. *Chem. Mater.* **2005** *17,* 5070.

[21]Abdul-Razzaq, W.; and Kouvel, J. S. Spin glassiness and ferromagnetism in disordered Ni-Mn (invited), *J. Appl. Phys.* **1984** *55,* 1623.

[22]Nam, D. N. H.; Jonason, K.; Nordblad, P.; Khiem, N. V.; and Phuc, N. X. Coexistence of ferromagnetic and glassy behavior in the $La_{0.5}Sr_{0.5}CoO_3$ perovskite compound. *Phys. Rev. B* **1999** 59, 4189.

[23]Asai, K.; Yokokura, O.; Nishimori, N.; Chou, H.; Tranquada, J. M.; Shirane, G.; Higuchi, S.; Okajima, Y.; and Kohn, K. Neutron-scattering study of the spin-state transition and magnetic correlations in $La_{1-x}Sr_xCoO_3$ (x=0 and 0.08). *Phys. Rev. B* **1994** *50*, 3025.

[24]Sánchez-Benítez, J.; Prieto, C.; de Andrés, A.; Alonso, J. A.; Martínez-Lope, M. J.; Casais, M. T. Evidence of two different states in $CaCu_3Mn_4O_{12}$ derivatives with colossal magnetoresistance. *Phys. Rev. B* **2004** *70,* 024419.

[25]Phan, M. H.; Yu, S. C.; Review of the magnetocaloric effect in manganite materials. *J. Magn. Magn. Mater.* **2007** *308,* 325.

[26]Korte, B. J.; Pecharsky, V. K.; Gschneidner, K. A. The correlation of the magnetic properties and the magnetocaloric effect in $(Gd_{1-x}Er_x)NiAl$ alloys. *J. Appl. Phys.* **1998** ***84,*** 5677.

[27]Gschneidner Jr., K. A.; Pecharsky, V. K.; Pecharsky, A. O.; Zimm, C. B. Recent developments in magnetic refrigeration. *Mater. Sci. Forum.* **1999** *315-317,* 69.

[28]Provenzano, V.; Shapiro, A. J.; Shull, R. D. Reduction of hysteresis losses in the magnetic refrigerant $Gd_5Ge_2Si_2$ by the addition of iron. Nature (London) **2004** *429,* 853.

[29]Kolano-Burian, A.; Szymczak, R; Kolano, R.; Szymczak, H.; Burian, A.; Hawełek, Ł.; Zackiewicz P.; and Czepelak, M. Magnetocaloric effect in polycrystalline La based manganites modified with Sr. *J. Phys.: Conf. Ser.* **2011** *303* 012070.

[30]Trung, N. T.; Ou, Z. Q.; Gortenmulder, T. J.; Tegus, O.; Buschow, K. H. J.; Brück, E. Tunable thermal hysteresis in MnFe(P,Ge) compounds. *Appl*. *Phys*. *Lett*., **2009** *94,* 102513.

[31]Phan, M. H.; Peng, H. X.; Yu, S. C.; Large magnetocaloric effect in single crystal $Pr_{0.63}Sr_{0.3}MnO_3$. *J. Appl. Phys.* **2005** *97,* 10M306.

[32]Phan, M.H.; Yu, S.C.; Hur, N.H. Excellent magnetocaloric properties of $La_{0.7}Ca_{0.3-x}Sr_xMnO_3$ ($0.05 \leqslant x \leqslant 0.25$) single crystals. *Appl. Phys. Lett.* **2005** *86* 072504.

[33]Shen, J.; Gao, B.; Dong, Q.Y.; Li, Y. X.; Hu, F. X.; Sun, J. R. Shen, B. G. Magnetocaloric effect in $La_{1-x}Pr_xFe_{10.7}Co_{0.8}Si_{1.5}$ compounds near room temperature. *J. Phys. D: Appl. Phys.* **2008** *41,* 245005.

TOC/Abstract Graphics

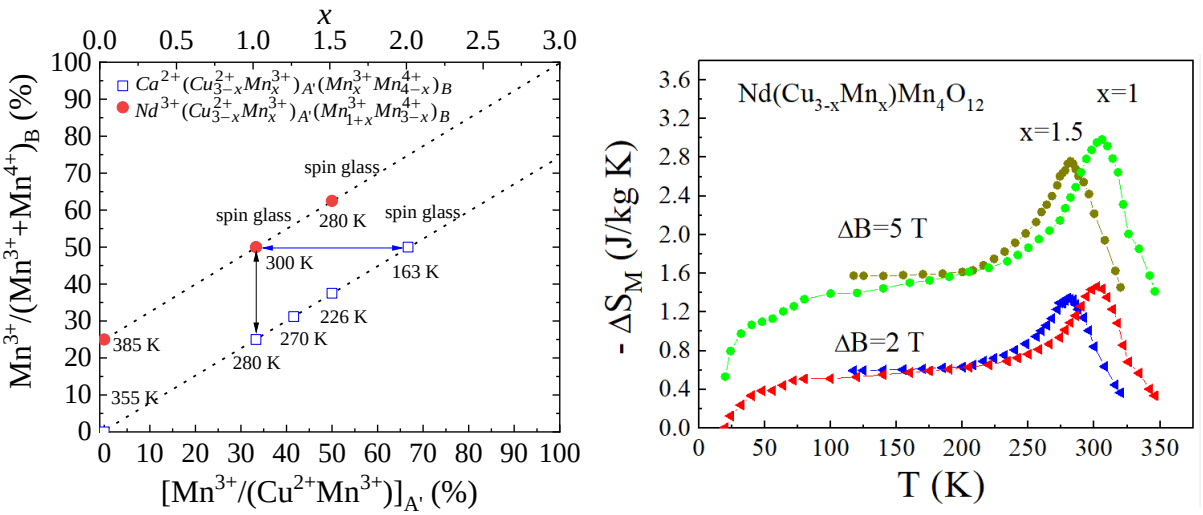

(Left) B-site $Mn^{3+}/(Mn^{3+}+Mn^{4+})_B$ ratio *versus* A'-site $Mn^{3+}/(Cu^{2+}+Mn^{3+})_{A'}$ ratio (bottom axis) and *x* value (top axis) in $Ln(Cu_{3-x}Mn_x)Mn_4O_{12}$ (Ln=Ca and Nd); (Right) Room temperature magnetocaloric effect in $Nd(Cu_{3-x}Mn_x)Mn_4O_{12}$ (x = 1 and 1.5) compounds